Tuning the band gap of hematite α-Fe_2O_3 by sulfur doping

Congxin Xia,[1, 2,*] Yu Jia,[1] Meng Tao,[3] Qiming Zhang[2]

[1]*Center for Clean Energy and Quantum Structures, and School of Physics and Engineering, Zhengzhou University, Zhengzhou, Henan 450001, China*

[2]*Department of Physics, University of Texas at Arlington, Arlington, Texas 76019, USA*

[3]*School of Electrical, Computer and Energy Engineering, Laboratory for Terawatt Photovoltaics, Arizona State University, Tempe, Arizona 85287, USA*

Abstract

Based on the density functional theory, the band structure and optical absorption of the isovalent sulfur-doped hematite α-Fe_2O_3 are studied systematically. The results show that the band gap of α-$Fe_2O_{3-x}S_x$ decreases monotonically with increasing the sulfur concentration, resulting in an obvious increase of the optical absorption edge in the visible range. Most intriguingly, unlike the pure α-Fe_2O_3 material, the α-$Fe_2O_{3-x}S_x$ with x≈0.17 (S concentration of ~5.6%) exhibits a direct band gap of an ideal value (~1.45 eV), together with high optical absorption (~10^5 cm^{-1}) and lower carriers effective masses. These results indicate that α-$Fe_2O_{3-x}S_x$, with a proper concentration of sulfur, may serve as a promising candidate for low-cost solar-cell materials.

Keywords: α-Fe_2O_3; isovalent doping; band structure; Optical absorption

---

* Corresponding author: Tel: 1-817-889-2998; Fax: 1-817-272-3637.

E-mail: cxia@uta.edu

1. Introduction

Hematite α-Fe_2O_3 has recently attracted extensive interests due to its favorable band gap (~2.1 eV) in the solar energy applications, which theoretically allows the utilization of approximately 40% of the solar spectrum [1-3]. In addition, it is a nontoxic, abundant, low-cost and environmentally friendly material. These are the necessary properties for massive applications of solar energy conversion at a competitive price [4]. However, the practical solar energy conversion efficiencies from the potentially low-cost material have been insufficient due to the poor performances, such as very short excited-state lifetime, relatively poor absorptivity and the indirect band gap [5, 6]. In order to utilize sunlight effectively, some research works have been done to change the electronic structures and transport properties of α-Fe_2O_3 by using controlled doping methods, such as the experimental studies involved in Al, Ti, Sn, Si, Cr and Mo [7-17] and the density functional theory (DFT) studies on Co, Cu, Pd, Nb, Al and Ti [16-23]. These studies show that although cation substitutional doping can improve the photocurrent in α-Fe_2O_3, the reported solar energy conversion efficiencies are still too low to make them applicable. Thus, in order to make use of α-Fe_2O_3 as high performance solar energy materials, it is necessary to explore other effective doping methods to improve the electronic structures and optical properties of α-Fe_2O_3.

It is well known that for the high efficient solar-cell materials, a direct band gap with the range of 1.3~1.6 eV that maximizes absorption of incident sunlight is highly desirable. However, the indirect band gap (~2.1 eV) and high carrier effective mass of α-Fe_2O_3 limits its solar energy utilization. Therefore, it is important to find an efficient way to modify the band structures near the band gap of α-Fe_2O_3. The cationic doping in α-Fe_2O_3 has been extensively studied both experimentally and theoretically [7-23], while there are few experimental and theoretical studies involved in anionic doping in α-Fe_2O_3 to date. The experimental studies of N-doped α-Fe_2O_3 show that a typical cathodic photocurrent originated from the *p*-type conduction was obtained, while the value of the indirect band gap of 1.96 eV indicates N doping scarcely affects the band structures and the energy gap of α-Fe_2O_3[24]. Most of these doping aimed to provide extra carriers to the material. Only the studies of the isovalent substituional doping by Al [16] aimed to modify the band gap and edges. But no significant changes were made. On the other hand, some very recent studies conclude that α-Fe_2O_3 has good hole transport properties [25, 26], which may draw much further attention to modify its valence band edges and *p*-type conduction for solar energy utilization because the upper valence band edge of α-Fe_2O_3 is dominated by O 2p states. To our best knowledge, such anionic isovalent doping in α-Fe_2O_3 has not yet been done.

In order to further understand how anionic isovalent doping affects the band structures and optical properties of α-Fe_2O_3, in this paper, we study the substitutional doping of sulfur on oxygen sites into α-Fe_2O_3 by means of the first-principles calculations based on DFT. We found that the band gap of α-$Fe_2O_{3-x}S_x$ decreases monotonically with increasing the *x*, resulting in an obvious increase of the optical absorption edge in the visible range. Furthermore, a direct band gap of an ideal value (~1.45 eV) could be achieved when the concentration of S is ~5.6% (at x=0.17). We hope our study can bring more interests on the further investigations of α-$Fe_2O_{3-x}S_x$ as a low-cost and high effective solar energy material.

2. Calculation methods

All the calculations performed in this work are based on spin-polarized DFT method as implemented in the Vienna *ab initio* simulation package (VASP) [27]. The exchange–correlation functional is treated within the generalized gradient approximation (GGA) and parameterized by Perdew-Burke-Ernzerhofer (PBE) formula [28]. Projected augmented wave (PAW) potential [29] is employed to describe the electron-ion potential and a kinetic energy cutoff of 400 eV is selected for the plane wave expansion. The valence electron configurations considered in this study are Fe ($3p^6 3d^7 4s^1$), O ($2s^2 2p^4$) and S ($3s^2 3p^4$). In order to consider more precisely the effect of the on-site Coulomb repulsion of Fe 3d electrons, the exchange–correlation energy is treated by the GGA+U

approach used by Dudarev *et al*.[30]. Integrations over the first Brillouin zone are performed using Monkhorst-Pack k-point grid [31]. The convergence for energy is chosen as 10^{-5} eV between two steps. The structural optimization is obtained until the Hellmann-Feynman forces acting on each atom is less than 0.005eV/Å. In our calculations, the lattice constants of the supercells are kept unchanged whenever a dopant is introduced. Our test shows that the change of the band gap due to the further optimization of the lattice constants is one order of magnitude smaller than the change caused by doping.

We use different α-Fe_2O_3 hosted supercells to simulate different sulfur concentrations of S in α-$Fe_2O_{3-x}S_x$. For x=0.04 (or ~1.4% of S), it can be obtained when one oxygen is substituted by one sulfur atom in the 120-atom superccell (2×2×1 of the 30-atom hexagonal cell). The x=0.06 (or ~2.1% of S) can be simulated using one sulfur to substitute one oxygen atom in the 2×2×2 rhombohedral α-Fe_2O_3 supercell with 80 atoms. Moreover, the x=0.17 (or ~5.6% of S) and x=0.33 (or ~11% of S) are simulated by substituting one and two oxygen atoms with sulfur in the 30-atom hexagonal cell, respectively. Among available doping sites of sulfur substituting oxygen, the structures with the lowest total energy are taken.

The imaginary part $\varepsilon_2(\omega)$ of the dielectric function could be calculated from the momentum matrix elements between the occupied

and unoccupied wave functions with the selection rules [32], and the real part $\varepsilon_1(\omega)$ of the dielectric function can be evaluated from imaginary part by Kramer-Kronig relationship. The optical absorption coefficient $\alpha(w)$ can be obtained as follows

$$\alpha(\omega) = \sqrt{2}\omega[\sqrt{\varepsilon_1^2(\omega) + \varepsilon_2^2(\omega)} - \varepsilon_1(\omega)]^{\frac{1}{2}}. \qquad (1)$$

3. Results and discussion

3.1 Electronic structures of pure α-Fe_2O_3

To check the applicability and accuracy of the GGA+U method and PAW potentials used in the study, the optimized structural parameters, band structures and density of states (DOS) of pure α-Fe_2O_3 are calculated. The modeled structure of pure α-Fe_2O_3 is a hexagonal cell with 12 Fe and 18 O atoms. For the GGA+U method, the choice of U=4 is chosen to optimize the calculated band gap, the lattice constant and the magnetic moment. In order to establish the best agreement of the calculated bulk properties with the experimental data, different nonmagnetic and magnetic phases are initially considered. Non-collinear magnetic effects were not taken into account. The global energy minimum is an antiferromagnetic (AFM) + – – + (along the hexagonal [001] axis) state, which agrees with the previous DFT calculations [16-22, 33-35] and experimental measurements under the Neel temperature of 948 K [36]. The calculated magnetic moment of each Fe atom is 4.15 μ_B agreed with

the recent HSE06 calculation (4.16 μ_B) [19]. The optimized lattice constants ($a = 5.044$ Å, $c = 13.739$ Å) are in excellent agreement with experimental values ($a = 5.035$ Å, $c = 13.747$ Å) [37]. In addition, Fig. 1 (a) shows that a pure α-Fe_2O_3 has an indirect band gap with the value of 2.05 eV and the conduction band minimum (CBM) lies at M point and the valence band maximum (VBM) lies between M and G points, which is very consistent with the previous calculated results [16,19]. Fig. 1 (b) shows that the upper edge of the valence band is dominated mainly by O 2p states, while the lowest conduction band edge is mainly Fe 3d states in character, which indicates that hematite α-Fe_2O_3 is a charge-transfer insulator, agreeing with the experimental spectroscopic measurements [29] and the previous theoretical studies [34,35]. The above calculated results justify our choice of the GGA+U method and the PAW potentials used throughout the following calculations. It is noted that in the present letter, only the spin-up band structures and DOS are plotted although the AFM states are kept in all the calculations. Even when the substitution of O atom by S is introduced, the AFM state is unchanged, although there is about 3% reduction of the magnetic moments at the nearest neighboring Fe atoms.

3.2 Electronic structures and optical absorptions of α-$Fe_2O_{3-x}S_x$

In order to search for the ideal band gap for solar cell applications by S substituting O atom, in Fig. 2, we calculate the band gap values of

different S concentrations of α-$Fe_2O_{3-x}S_x$. Numerical results show that the band gap value is decreased monotonically when sulfur concentration (or the x values) is increased, which indicates that sulfur substituting oxygen can narrow effectively the band gap value of hematite α-Fe_2O_3. This trend is consistent to what was reported very recently in iron pyrite (FeS_2)[38], where the band gap increases when O was introduced to replace S. Both cases improve the band gaps of their materials for solar energy applications. In particular, the band gap values of α-$Fe_2O_{3-x}S_x$ are found to be 1.45 eV and 1.28 eV with x=0.17 and x=0.33, respectively. These band gap values are optimal to the visible optical absorption for solar cells. Thus, in the following, we will focus on the study of the band structures, optical absorptions and formation energies of α-$Fe_2O_{3-x}S_x$ with x=0.17 and x=0.33.

Fig. 3 presents the band structures of the α-$Fe_2O_{3-x}S_x$ with x=0.17 and x=0.33. We can find from Fig. 3(a) that at x=0.33, the VBM is very close to M point and the CBM lies at M point. In particular, Fig. 3(b) also shows that at x=0.17, the VBM and CBM are both located at M point which means that the band structures are tuned into the direct band gap. For this kind of transformation of the band structure and the energy gap, it means a significant advantage for the effective optical absorption and hence a better performance for solar cells. Moreover, we can find from Fig. 3 that compared to the band structure of pure α-Fe_2O_3, the curvature

at VBM of α-$Fe_2O_{3-x}S_x$ with x=0.17 increases, indicating a faster moving velocity of photo-generated holes. The calculated electron and hole effective masses of α-$Fe_2O_{3-x}S_x$ with x=0.17 (or ~5.6% of S) are 1.3 m_e and 1.6 m_e, about 19% and 26% lower than that of the pure α-Fe_2O_3, respectively. Our calculated electron and hole effective masses are 1.6 m_e and 2.17 m_e for the pure α-Fe_2O_3, in good agreement with the previous GW calculation results [39] of 1.5 m_e and 2.1 m_e, respectively. The lower effective masses will enhance the mobility of carriers in α-Fe_2O_3 and improve the conductivity.

To understand the origin of the band-gap narrowing of α-Fe_2O_3 due to isovalent sulfur substitution, the projected density of states (PDOS) of α-$Fe_2O_{3-x}S_x$ with x=0.17 and x=0.0 (pure) are compared in Fig. 4. The zero of energy is chosen at the top of the occupied bands of the pure α-Fe_2O_3, while the energy levels of the S-doped material are aligned with the pure one through the 1s core level of the same remote oxygen atom in both calculations. The top of the valence bands are dominated by O 2p and Fe 3d states while the bottom of the conduction bands are mainly Fe 3d states, as shown in Fig.1. Since S 3p orbitals are larger spacially than O 2p orbitals, the interaction with the orbitals of other atoms, especially its neighbors, will be increased after the substitution. The stronger interaction broadens the top valence bands, that are dominated by Fe 3d and O 2p, causing the reduction of the gap. As shown in Fig. 4, the

contribution to the broadening of the valence bands comes not only from the doped S 3p state, but also from O 2p and Fe 3d states. On the other hand, the bottom of the conduction bands is basically unchanged after S-doping. The analysis of PDOS for each atom in the cell shows that these changes are more obvious for the nearest-neighbor Fe and O atoms around the S atom. After all, the mixing of the S 3p states with the valence band top edge increases the width of the valence bands, resulting in a decrease in the band gap of the α-$Fe_2O_{3-x}S_x$. As a result, these changes lead to a decrease of the threshold for photon excitation energy and induce more significant red shift of optical absorption.

In Fig. 5, we further present the optical absorption variations for different S concentrations in α-$Fe_2O_{3-x}S_x$. Numerical results show that for the pure α-Fe_2O_3 case, the optical absorption coefficient approaches to zero when the wavelength lies within the 600~800 nm. However, after the S substituting O atom in α-Fe_2O_3, the red shift of the absorption edge and the increasing of the absorption strength can be observed easily in the visible light activity range. These results show that the anionic sulfur doping is an efficient way to enhance visible light activity for α-Fe_2O_3.

3.3 Formation energies for Sulfur-doped α-Fe_2O_3

The availability of the isovalent sulfur substitution in hematite α-Fe_2O_3 with different sulfur-doping levels have been investigated by calculating the formation energies of the α-$Fe_2O_{3-x}S_x$ according to the formula

$$E_{form} = E(doped) - E(pure) - n\mu_S + n\mu_O , \qquad (2)$$

where *E*(doped) and *E*(pure) are the total energies of S-doped and pure α-Fe_2O_3 supercells, respectively. μ_O and μ_S denote the chemical potentials of sulfur and oxygen atoms, respectively. *n* is the number of the sulfur atoms in substitution of the oxygen atoms. It should be noted that the formation energy depends on growth conditions, which may vary between the O-rich and the Fe-rich conditions. Under the Fe-rich condition, the Fe is assumed in thermodynamic equilibrium with bulk solid phase and its chemical potential μ_{Fe} is assumed to be the energy of one atom in bulk Fe. μ_O can be obtained according to the relationship

$$2\mu_{Fe} + 3\mu_O = \mu_{Fe_2O_3} , \qquad (3)$$

where $\mu_{Fe_2O_3}$ is the total energy of one formula hematite α-Fe_2O_3. Under the O-rich environment, the O into the hematite α-Fe_2O_3 is assumed to be in equilibrium with O_2 gas and μ_O can be obtained from the ground-state total energy of the O_2 molecule ($\mu_O = 1/2\,\mu(O_2)$), while the μ_{Fe} is fixed by Eq. (3). The chemical potential μ_s is calculated from the pyrite FeS_2 ($\mu_{FeS_2} = \mu_{Fe} + 2\mu_s$), assuming the co-existence of it during the growth. In order to avoid the formation of Fe_3O_4, the Fe and O chemical potential satisfy the relation $3\mu_{Fe} + 4\mu_O \le \mu_{Fe_3O_4}$ .The calculated formation energies are around 2.8 (0.78) eV per sulfur substitution under the O-rich (Fe-rich) conditions, which indicates that it is energy favorable and relatively easier to incorporate sulfur atom into the α-Fe_2O_3 under Fe-rich condition.

It could be a challenge to synthesize $Fe_2O_{3-x}S_x$, especially at a high S concentration since there exists no isostructural crystal iron sulfide. But at the concentration of ~5.6% of S, the synthesis is still feasible. The similar doping concentration of S in TiO_2 has been experimentally reported [40].

4. Conclusion

In conclusion, we have investigated the electronic structures and optical properties of isovalent sulfur substitution of oxygen in the α-Fe_2O_3 by means of the first-principles calculations. It is found that the substitution of sulfur for oxygen atom can cause a significant change in the band gap, band edges and optical absorption of the α-Fe_2O_3. The calculated band gap of the α-$Fe_2O_{3-x}S_x$ decreases monotonically with the increment of sulfur concentration, which results in an obvious increase in the visible activity range of the optical absorption edge. In particular, the α-$Fe_2O_{3-x}S_x$ with x=0.17 (~5.6% of S) has a direct band structure with the band gap value of 1.45 eV and lower carrier effective masses. Our results also indicate that sulfur substituting oxygen atom in α-Fe_2O_3 is relatively easier under the Fe-rich condition. These results are interesting and may shed light on a further experimental investigation of the α-$Fe_2O_{3-x}S_x$ as a low-cost and high effective solar energy material. The experimental investigation has been started in our group [41].

Acknowledgments

We thank Muhammad N. Huda for beneficial discussions. This research was supported by the U.S. Department of Energy, Office of Basic Energy Sciences, Division of Materials Sciences and Engineering under Award No. DE-SC0002062. Y. Jia thank the support by “973 project” (No.2012C13921300) and the NSF of China (No.11274280). The computational work was done at the High Performance Computing Center of the University of Texas at Arlington and the Texas Advanced Computing Center (TACC) at the University of Texas at Austin.

References

[1] M. Barroso, A. J. Cowan, S. R. Pendlebury, M. Gratzel, D. R. Klug, J. R. Durrant, J. Am. Chem. Soc. 133 (2011) 14868.

[2] M.F. Al-Kuhaili, M. Saleem, S.M.A. Durrani, J. Alloys Compd. 521 (2012) 178.

[3] A. Kiejna, T. Pabisiak, J. Phys. Condens. Matter. 24 (2012) 095003.

[4] A. Hellman, R. G. Pala, J. Phys. Chem. C 115 (2011) 12901.

[5] L.Yichuan, G.Wang, D. A. Wheeler, J. Zhang, Y. Li, Nano Lett. 11 (2011) 2119.

[6] I. Cesar, K. Sivula, A. Kay, R. Zboril, M. Gratzel, J. Phys. Chem. C 113 (2009) 772.

[7] M. Gaudon, N. Pailhe, J. Majimel, A.Wattiaux, J. Abel, J. Solid State. Chem. 183 (2010) 2101.

[8] N. T. Hahn, C. B. Mullins, Chem. Mater. 22 (2010) 6474.

[9] M. A. Lukowski, S. Jin, J. Phys. Chem. C 115 (2011) 12388.

[10] A. Kleiman-Shwarsctein, Y. S. Hu, A. J. Forman, G. D. Stucky, E. W. McFarland, J. Phys. Chem. C 112 (2008) 15900.

[11] A. Kay, I. Cesar, M. Gratzel, J. Am. Chem. Soc. 128 (2006) 15714.

[12] S. S. Shinde, C. H. Bhosale, K. Y. Rajpure, J. Alloys Compd. 509 (2011) 3943.

[13] G. K. Reddy, K. Gunasekera, P. Boolchand, J. H. Dong, P. G. Smirniotis, J. Phys. Chem. C 115 (2011) 7586.

[14] M. Zhang, W. Luo, Z. Li, T. Yu, Z. Zou, Appl. Phys. Lett. 97 (2010) 042105.

[15] J. Liu, C. Liang, H. Zhang, Z. Tian, S. Zhang, J. Phys. Chem. C 116 (2012) 4986.

[16] A. Kleiman-Shwarsctein, M. N. Huda, A. Walsh, Y.Yan, G. D. Stucky, Y. S. Hu, M. M. Al-Jassim, E. W. McFarland, Chem. Mater. 22 (2010)510.

[17] T. Droubay, K. M. Rosso, S. M. Heald, D. E. McCready, C. M. Wang, S. A. Chambers, Phys. Rev. B. 75 (2007) 104412.

[18] X. Y. Meng, G. W. Qin, S. Li, X. H. Wen, Y. P. Ren, W. L. Pei, L. Zuo, Appl. Phys. Lett. 98 (2011) 112104.

[19] Z. D. Pozun, G. Hekelman, J. Chem. Phys. 134(2011)224706.

[20] C. S. Praveen, V. Timon, M. Valant, Computat. Mater. Sci. 55 (2012) 192.

[21] A. Bandyopadhyay, J. Velev, W. H. Butler, S. K. Sarker, O. Bengone, Phys. Rev. B 69 (2004) 174429.

[22] R. Rivera, H. P. Pinto, A. Stashans, L. Piedra, Phys. Scr. 85 (2012) 015602.

[23] H. Tang, W. Yin, M. A. Matin, H. Wang, T. Deutsch, M. M. A. Jassim, J. A. Turner, Y. Yan, J. Appl. Phys. 111 (2012) 073502.

[24] T. Morikawa, K. Kitazumi, N. Takahashi, T. Arai, T. Kajino, Appl. Phys. Lett. 98 (2011) 242108.

[25] H. Peng, S. Lany, Phys. Rev. B 85(2012) 201202(R).

[26] P. Liao, E. A. Carter, J. Appl. Phys. 112 (2012) 013701.

[27] G. Kresse, J. Furthmüller, Phys. Rev. B 54 (1994) 11169.

[28] J. P. Perdew, J. A. Chevary, S. H.Vosko, K. A. Jackson, M. R. Pederson, D. J. Singh, C. Fiolhais, Phys. Rev. B 46 (1992) 6671.

[29] G. Kresse, D. Joubert, Phys. Rev. B 59 (1999)1758.

[30] S. L. Dudarev, G. A. Botton, S.Y. Savrasov, C. J. Humphreys, A. P. Sutton, Phys. Rev. B 57(1998)1505.

[31] G. Drager, W. Czolbe, J. A. Leiro, Phys. Rev. B 45 (1992) 8283.

[32] M. Gajdos, K. Hummer, G. Kresse, J. Furthmuller, F. Bechstedt, Phys. Rev. B 73 (2006) 045112.

[33] N. C. Wilson, S. P. Russo, Phys. Rev. B 79 (2009) 094113.

[34] P. Canepa, E. Schofield, A. V. Chadwick, M. Alfredsson, Phys. Chem. Chem. Phys. 13 (2011) 12826.

[35] L. M. Sandratskii, M. Uhl, J. Kubler, J. Phys.: Condens. Matter 8 (1996) 983.

[36] A. H. Morrish, Canted Antiferromagnetism: Hematite, World Scientific, Singapore, 1994.

[37] L. W. Finger, R. M. Hazen, J. Appl. Phys. 51(1980) 5362.

[38] J. Hu, Y. Zhang, M. Law, R. Wu, J. Am. Chem. Soc. 134 (2012) 13216.

[39] H. Peng and S. Lany, Phys. Rev. B 85, (2012) 201202(R).

[40] W. Ho, J. C. Yu, S. Lee, J. Solid State Chem. 179 (2006) 1171.

[41] X. Han, B. Zhou, M. Tao, *Proceedings of 38th IEEE Photovoltaic Specialists Conference*, Austin, 2012.

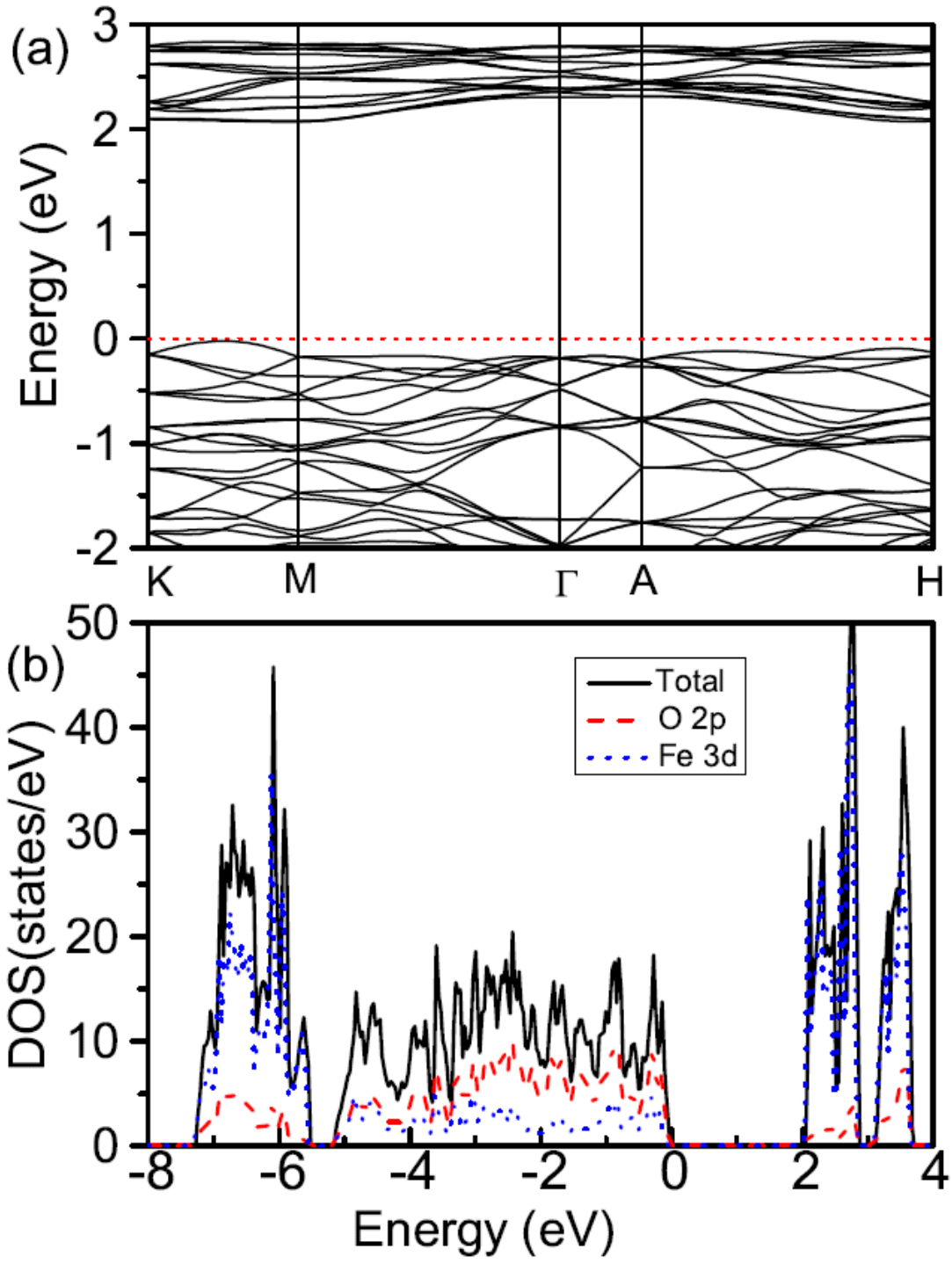

Fig. 1. The spin-up band structure (a) and densities of states (DOS) (b) of pure hematite α-Fe_2O_3 in 30-atom hexagonal cell. The zero of energy is chosen as the highest occupied band (dashed line).

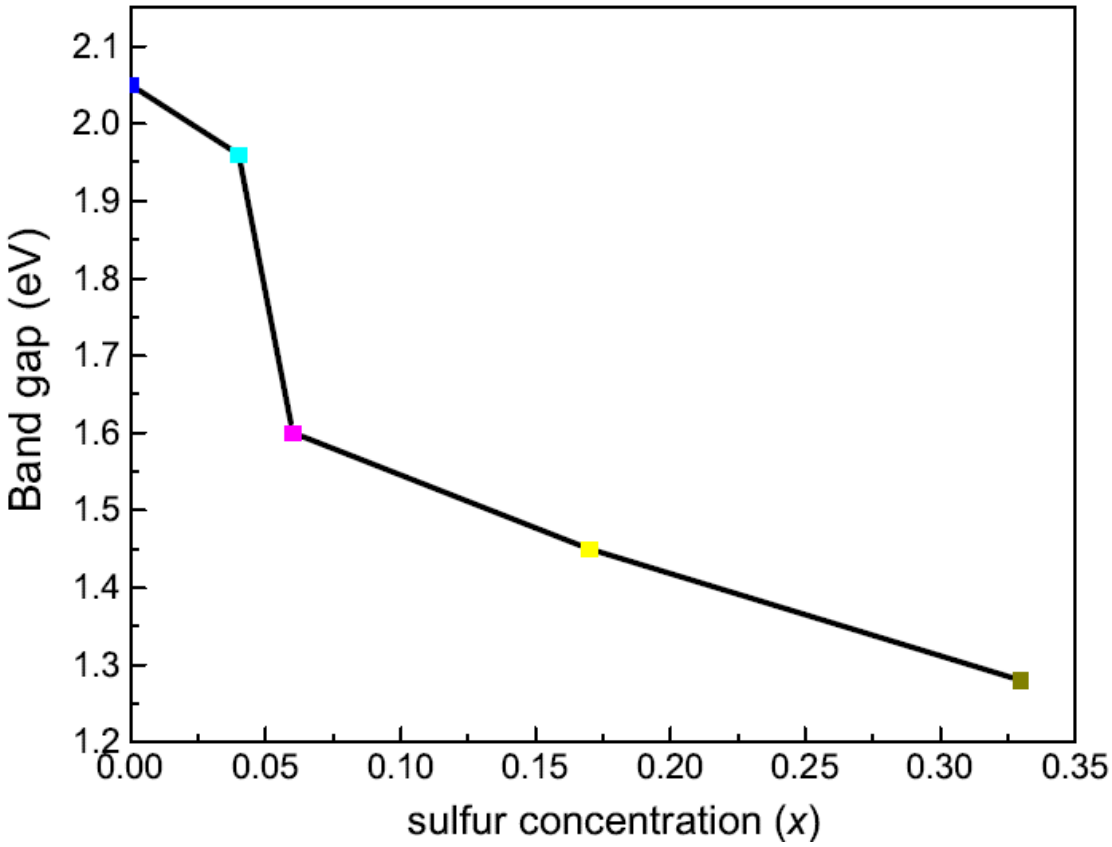

Fig.2. The calculated band gap values as a function of x in α-$Fe_2O_{3-x}S_x$. Different square marks are the band gap values of x=0, 0.04, 0.06, 0.17 and 0.33 , corresponding to the sulfur concentration of 0%, 1.4%, 2.1%, 5.6% and 11%, respectively.

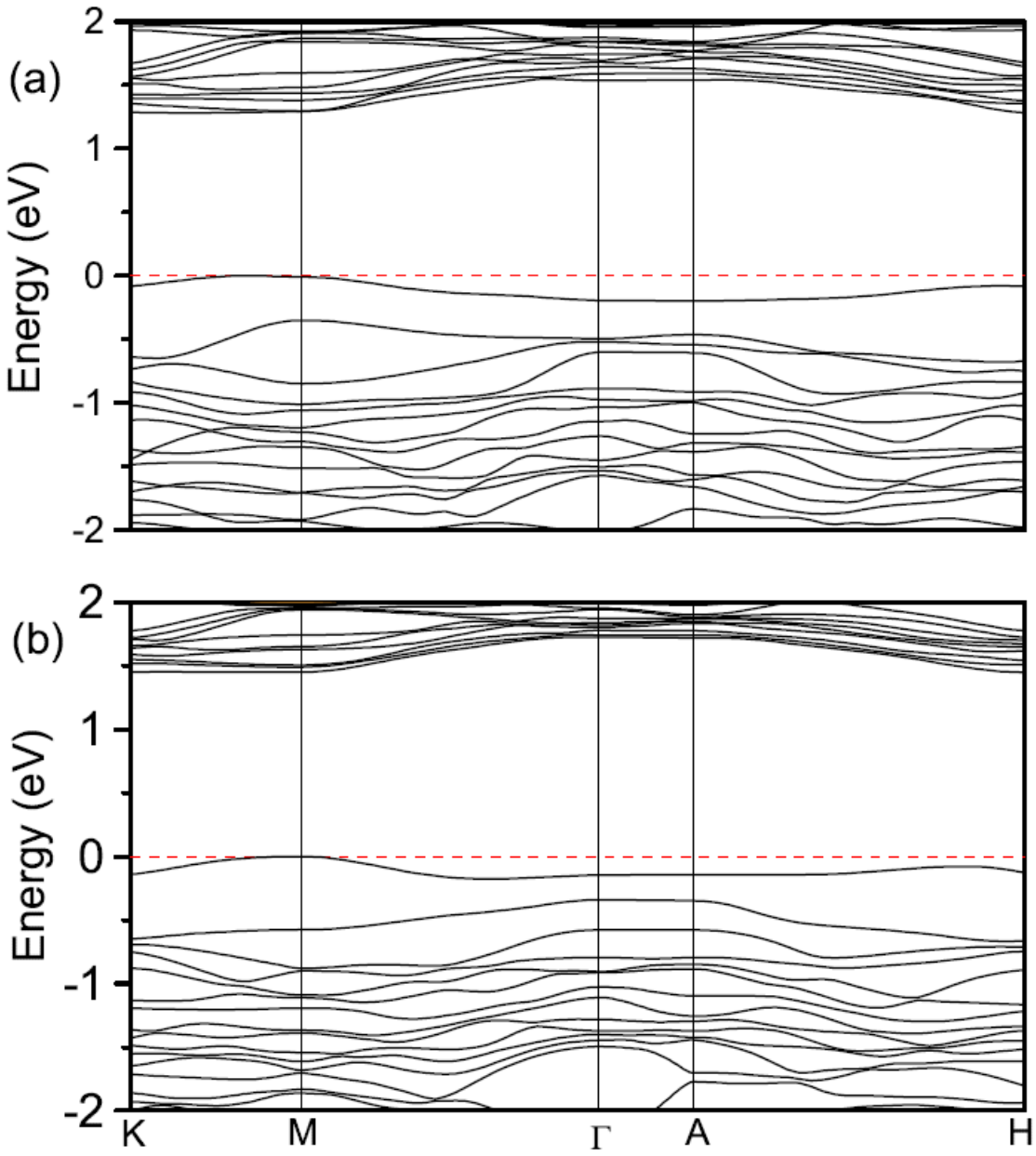

Fig.3. The spin-up band structures of α-$Fe_2O_{3-x}S_x$ with x=0.33 (a) and x=0.17 (b). The zero of energy is chosen as the highest occupied band (dashed line).

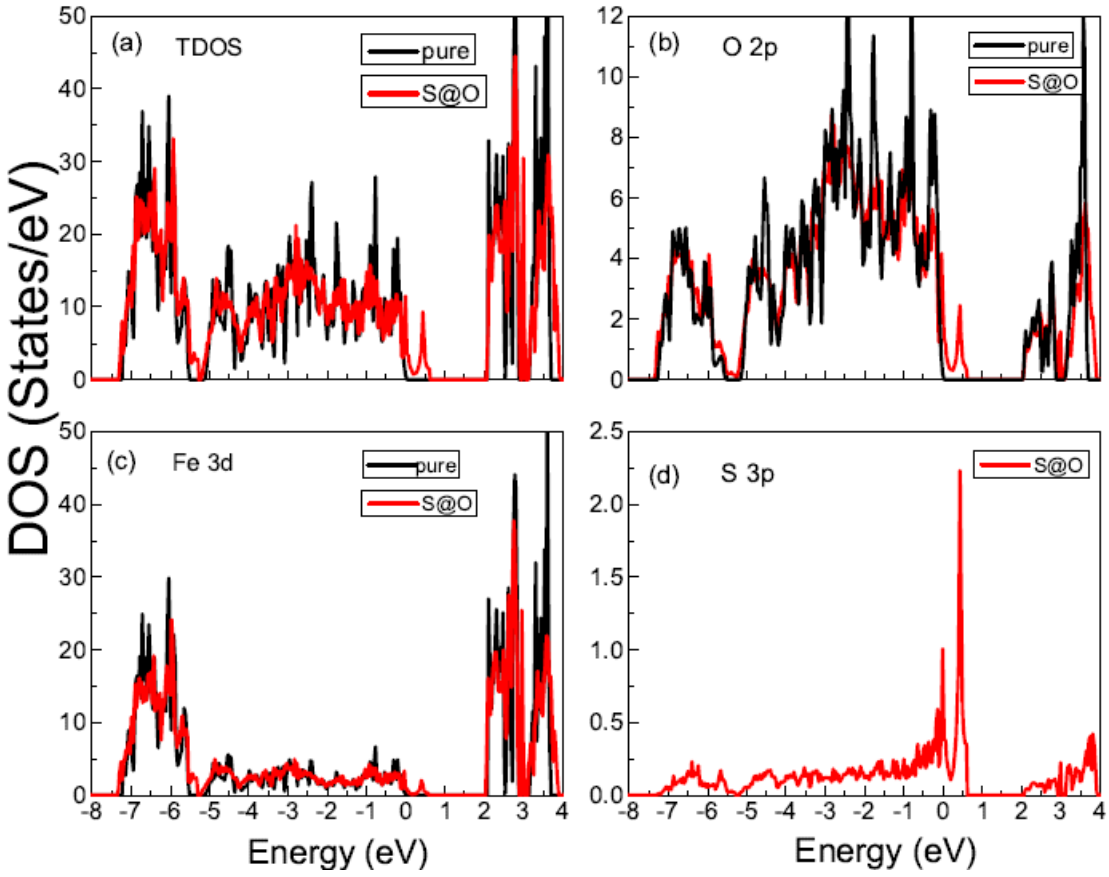

Fig. 4. The total density of states (TDOS) (a), the O 2p (b), Fe 3d (c) and S 3p (d) projected density of states (PDOS) of hematite α-$Fe_2O_{3-x}S_x$ with x=0.0 (black line) and x=0.17 (red line). The zero of energy is chosen at the top of the occupied bands of the pure α-Fe_2O_3. The S-doped lines are aligned with the pure ones with respect to the O 1s core level. Only the spin-up parts are shown.

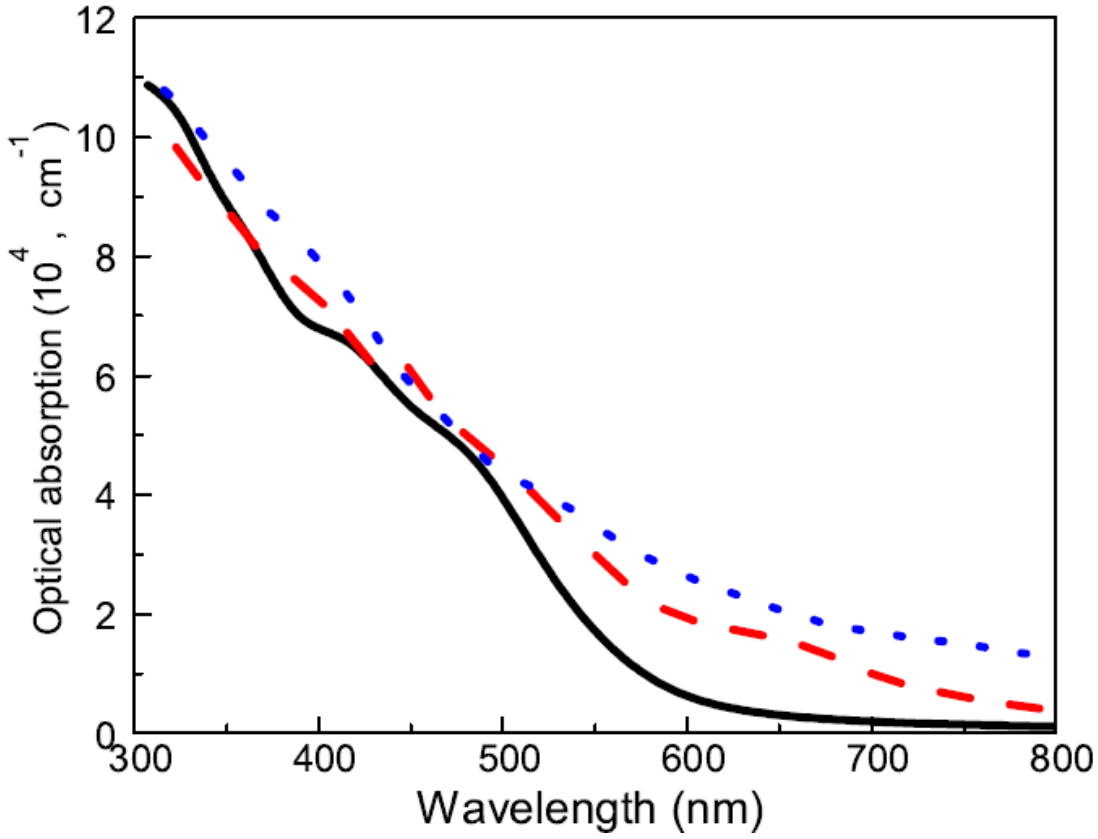

Fig. 5. The optical absorption coefficient as a function of the wavelength. The black solid line, red dashed line and blue dotted line are for x=0, x=0.17 and x=0.33, respectively, in α-$Fe_2O_{3-x}S_x$.